ACS OMEGA

http://pubs.acs.org/journal/acsodf

Article

Improved Perovskite/Carbon Interface through Hot-Pressing: A Case Study for $CsPbBr_3$-Based Perovskite Solar Cells

Teng Zhang,*,# Chengben Liu,# Zhi Li, Baohua Zhao, Youru Bai, Xinmei Li, Wenwen Liu, Yanli Chen, Zhaobin Liu, and Xiyou Li*

Cite This: *ACS Omega* 2022, 7, 16877−16883

Read Online

ACCESS | Metrics & More | Article Recommendations | Supporting Information

ABSTRACT: Due to the low cost and printable nature of the carbon paste, carbon-based perovskite solar cells (PSCs) are attractive for real application. However, the poor contact at the perovskite/carbon interface obviously hinders the achievable fill factor of the carbon-based PSCs. In this work, we introduce a pressure-assisted method to improve the contact at the perovskite/carbon interface. Via modulating the applied pressure, the power conversion efficiency of $CsPbBr_3$ PSCs (small area) can be improved from the initial 7.40% to 7.95% (pressing) and 8.34% (hot-pressing). A more remarkable feature is that the hot-pressing process boosted the performance from 5.1% (normal) to 6.9% (hot-pressing assisted) of large-scale (0.5 cm^2) devices, a more than 30% enhancement. Finally, the hot-pressing method introduced in this work shows great prospects for improving the efficiency of carbon-based PSCs, especially large-scale PSCs.

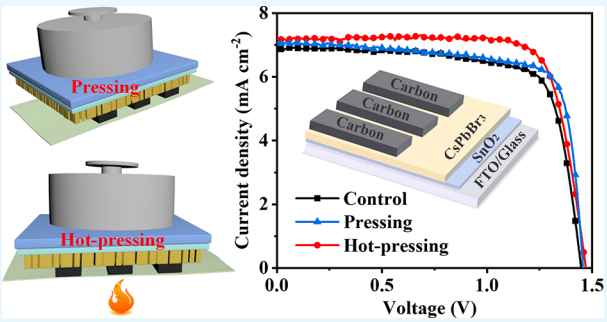

INTRODUCTION

Benefited from their excellent optical and electrical properties, organic−inorganic metal halide perovskite solar cells (PSCs) have attracted great attention among both academic and industrial fields.[1−5] Meanwhile, conventional PSCs use noble 2,2′,7,7′-tetrakis[*N*,*N*-di(4-methoxyphenyl)amino]-9,9′-spirobifluorene (Spiro-OMeTAD) and costly metal electrodes, which reduce the cost-effectiveness of PSCs. Carbon-based PSCs, which exclude hole transport materials and replace the metal electrode with carbon paste, turn out to be an alternative option. To start with, Han et al. first demonstrated the carbon-based PSCs with a device structure of FTO/TiO_2/ZrO_2/perovskite/carbon.[6] Yang et al. later suggested that candle soot can be an excellent hole extraction layer for PSCs.[7] Subsequently, multiple carbon materials including graphite,[8−10] carbon black,[11,12] spongy carbon,[13] and carbon cloth[14] are developed for PSC application. Very recently, the power conversion efficiencies (PCEs) of carbon-based HTL-free PSC have been boosted to 18.9%,[15] and fully printed planar carbon-based PSCs shows a record PCE of 15.3%.[16]

Although progressive achievements have been reached for carbon-based PSCs, the record efficiency (18.9%) is far lower than that of conventional PSCs (25.5%).[17] This is largely due to the poor contact at the perovskite/carbon interface. To be more specific, because the carbon paste is composed of a graphite flake and carbon sphere, pinholes are unavoidable at the perovskite/carbon interface. This results in pronounced photo-carrier recombination. Several researchers have demonstrated a better adhesion at the perovskite/carbon interface-promoted carrier transportation.[18−25] Then, interface engineering turns out to be an effective strategy for enhancing the performance of carbon-based PSCs. Materials including inorganic compounds (MnS[26] and Mxene[27]) and organic materials (PEDOT, PPy, PANi,[28] CuPc,[29] hexamethylenetetramine,[30] and 1-butyl-2, 3-dimethylimidazolium chloride ([BMMIm]Cl) ionic liquids (ILs)[31]) are introduced to improve the interface contact and promote charge extraction. Yang et al. introduced cesium acetate (CsAc) at the perovskite/carbon interface, contributing to an improved V_{OC}.[25] What is more, formula engineering of the carbon paste also results in a better contact of the perovskite/carbon interface.[32−36] Although the aforementioned methods are attractive, they do not change the fluffy nature of the carbon layer.

In this study, we propose a simple hot-pressing method to solve the poor contact issue at the perovskite/carbon interface. $CsPbBr_3$ has been selected as the photoactive layer because the PCEs of carbon-based $CsPbBr_3$ PSCs are comparable or even superior to those of conventional metal electrode-structured devices.[37−39] After pressure treatment, the pinhole-free perovskite/carbon interface with reduced carbon layer thickness

Received: October 31, 2021
Accepted: January 17, 2022
Published: May 11, 2022

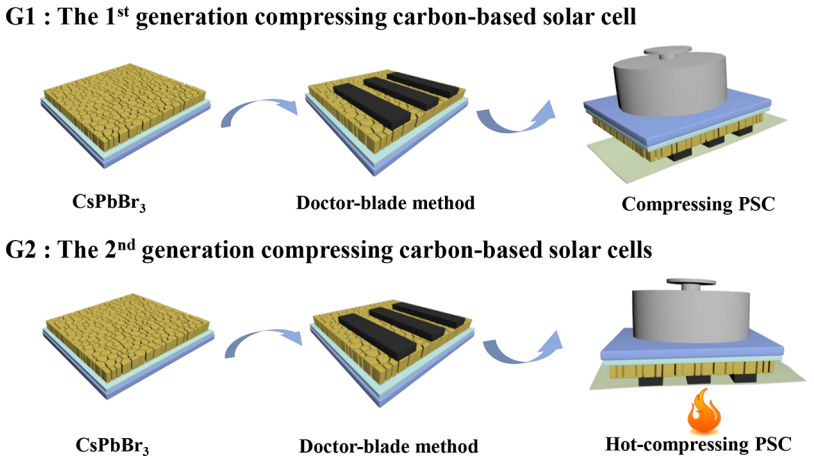

Figure 1. Schematic diagram of (G1) the pressing process and (G2) the hot-pressing process.

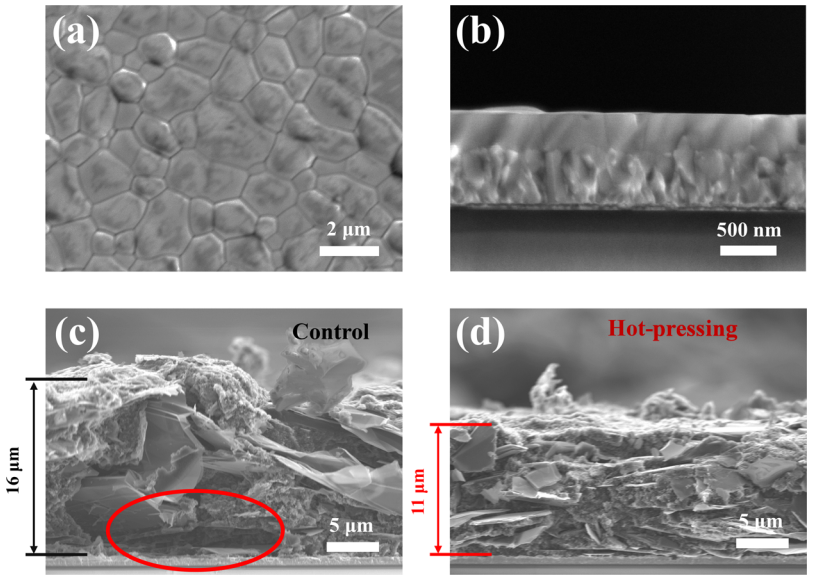

Figure 2. (a) Top-view SEM images of the $CsPbBr_3$ films deposited on the SnO_2/FTO substrate. (b) Cross-sectional SEM images of the $CsPbBr_3$ films. Cross-sectional SEM images of (c) the control device and (d) the hot-pressing device.

suggests an enhanced interfacial contact, benefiting the carrier extraction. We receive a PCE of 8.34% for hot-pressing-treated PSCs, compared with 7.4% of the control devices. Moreover, the method works better for large scale devices. PCE of large-scale devices has been increased by ∼30% (5.1% to 6.9%) after the hot-pressing treatment. Finally, thanks to the dense carbon layer after the hot-pressing process, the hot-pressing-treated PSCs also show improved stability at ambient conditions. After all, the hot-pressing method seems to be an effective method for developing high-efficiency, reproducible, and stable carbon-based PSCs.

RESULTS AND DISCUSSION

We start by describing the device fabrication process. The main difference of the device fabrication lies in the deposition of the carbon electrode. For the control devices, the commercial carbon paste is doctor-blade coated on the $CsPbBr_3/SnO_2$/FTO substrates and heated at 100 °C for 20 min. The pressing process refers to applying pressure to the fabricated devices at ambient conditions (Figure 1 G1). Meanwhile, the hot-pressing process suggests adding pressure on devices during the annealing process of the carbon paste (Figure 1 G2). The experimental details are listed in the Supporting Information. The influence of the G1 and G2 processes will be discussed later.

As for the $CsPbBr_3$ film fabrication, we use the methanol process developed by Tang et al.[33,40,41] The phase transition between $CsPb_2Br_5$, $CsPbBr_3$, and Cs_4PbBr_6 can be tuned by adjusting the spin-coating cycle of the CsBr precursor. With an optimized spin-coating cycle (8), the prepared films show diffraction peaks at 2θ = 15.2°, 21.6°, 30.7°, and 44.1° on the XRD spectrum, corresponding with the (100), (110), (200), and (220) lattice planes of the $CsPbBr_3$ phase, respectively (Figure S1). No additional peak showed up, which suggested the phase pure nature of the prepared films. The UV−vis absorption spectrum shows a distinct absorbance at ∼540 nm. This also supports the high quality of the prepared $CsPbBr_3$ films (Figure S2).

The SEM images illustrate that the prepared films are polycrystalline with a crystal size of ∼2 μm (Figure 2a). Grain boundaries are distinct, and pinholes can hardly be visible, which support the high quality of the prepared films. The average thickness of the prepared films is about 400−500 μm,

https://doi.org/10.1021/acsomega.1c06108
ACS Omega 2022, 7, 16877−16883

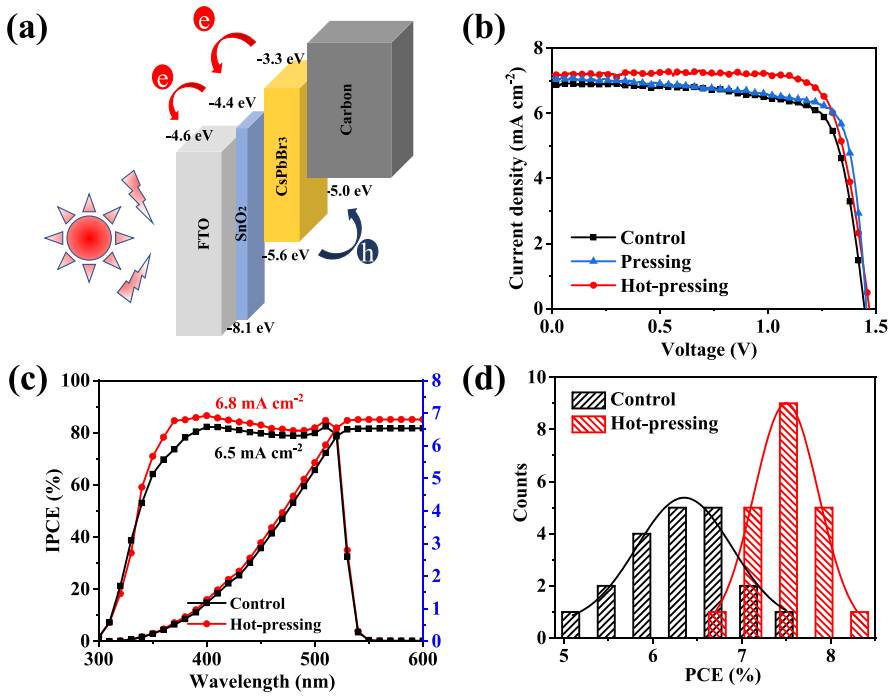

Figure 3. (a) Band alignment diagram of the $CsPbBr_3$ PSCs. (b) $J-V$ characterization of the PSCs. The $J-V$ curves have been measured at 0.1 V/s. (c) IPCE spectrum and the integrated J_{SC} calculated from the IPCE spectrum of the prepared $CsPbBr_3$ PSCs. (d) Histogram of the PCE values for PSCs prepared from different processes. Twenty devices were collected.

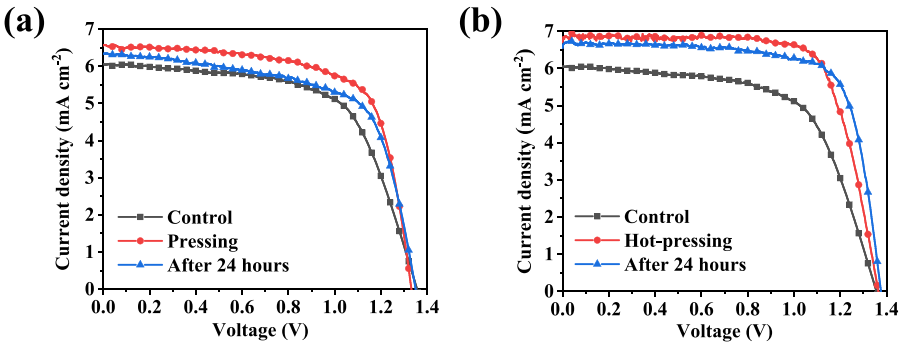

Figure 4. $J-V$ characterization of the large scale (0.5 cm^2) PSCs prepared with (a) pressing process and (b) hot-pressing process. The $J-V$ curves are measured under AM 1.5G one sun illumination (100 mW/cm^2) with a scan rate of 0.1 V/s.

consistent with the previous research (Figure 2b).[42] We are more interested in the morphological transformation of the carbon electrode layer before and after pressing. Listed in Figure 2c, the thickness of the carbon electrode layer for the control devices is ~16 μm, whereas this has been reduced to 11 μm for the hot-pressing devices, an almost 1/3 shrinkage. Moreover, shown on the side-view SEM images, there are obvious cracks and un-touched areas at the perovskite/carbon interface (marked in red), pointing to a poor contact (Figure 2c). Meanwhile, the hot-pressing carbon films show that the graphite flakes in the carbon paste are horizontally aligned, and the carbon electrode and the perovskite layer are tightly connected (Figure 2d); thus, effective carrier transportation can be guaranteed.

Next comes to the performance characterization. Under light illumination, the generated photo-electrons flow from the photo-active layer ($CsPbBr_3$) down to SnO_2 and are collected by the FTO substrate. The reverse is the case for the photo-holes (Figure 3a). As shown in Figure 3b and Table S1, the control device received an open-circuit voltage (V_{OC}) of 1.45 V, a short circuit current (J_{SC}) of 6.80 mA cm^{-2}, a fill factor (FF) of 0.75, and an overall power conversion efficiency (PCE) of 7.4%. This PCE has been increased from 7.40% to 7.93% (pressing) and 8.34% (hot-pressing). The integrated photocurrents calculated from the incident photon-to-electron conversion efficiency (IPCE) are 6.50 mA cm^{-2} (control) and 6.80 mA cm^{-2} (hot-pressing treated). The results are in good agreement with the J_{SC} measured from the $J-V$ characterization (Figure 3c, Table S1). After introducing the pressure-assisted process, the performance enhancement is mainly due to an improved J_{SC} (from 6.80 mA cm^{-2} to 7.18 mA cm^{-2}) and FF (from 0.75 to 0.79), corresponding well with a better contact at the selective interface. As for the reproducibility of the devices, 20 devices are selected for control and hot-pressing-treated process separately. The corresponding statistical histogram is provided in Figure 3d. The control devices yield a PCE of only 5–7%. In comparison, most of the hot-pressing-treated devices receive a PCE over 7%. Meanwhile, photocurrent hysteresis for the control and hot-pressing-treated devices is analyzed by the $J-V$ curves (Figure S3 and

https://doi.org/10.1021/acsomega.1c06108
ACS Omega 2022, 7, 16877−16883

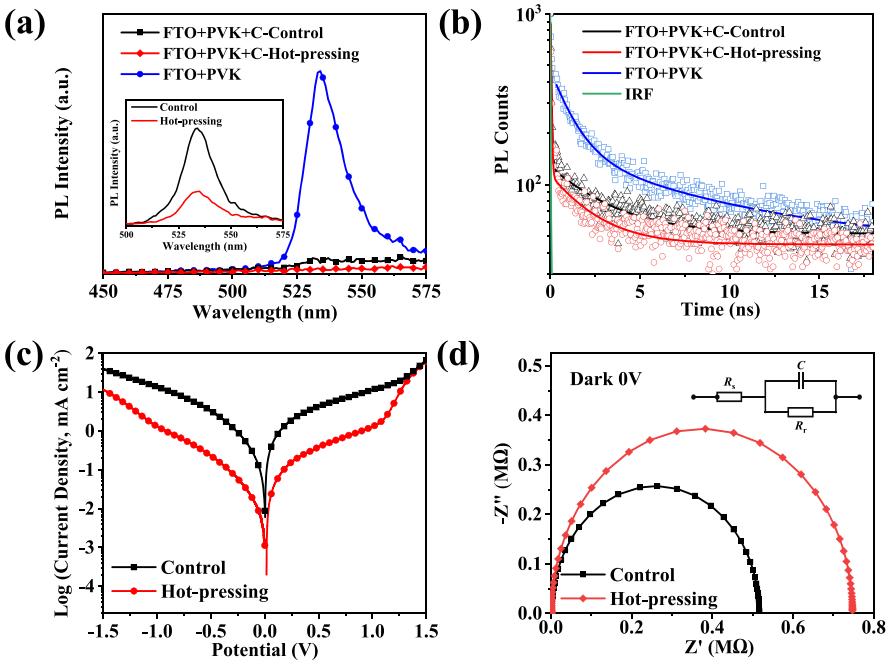

Figure 5. (a) Steady-state PL spectrum of the perovskite films. The measurements are conducted under a beam of 400 nm laser illuminated from the FTO side. (b) TRPL decay curves of the perovskite films deposited on the FTO substrate. A 405 nm laser is illuminated from the FTO side. IRF refers to the instrument response function. (c) Dark $J-V$ curves of the symmetrical FTO/perovskite/carbon structure. The $J-V$ curves are measured under dark conditions with a scan rate of 0.1 V/s. (d) Nyquist plots of the as-prepared perovskite solar cells in the dark at 0 V.

Table S2). Following previous reports,[43] photocurrent hysteresis can be expressed by the photocurrent hysteresis index (HI), which can be calculated as follows:

$$\mathrm{HI} = \frac{\mathrm{PCE}_{\mathrm{reverse}} - \mathrm{PCE}_{\mathrm{forward}}}{\mathrm{PCE}_{\mathrm{reverse}}}$$

The HI of the hot-pressing-treated devices is 6.8%, which is lower than that of the control devices (14.9%), indicating a reduced defect and an enhanced contact at the interface between the carbon and perovskite layer. Besides, the hot-pressing-treated devices also show a narrow PCE distribution (Figure 3d). These results indicate the advantages of the hot-pressing process.

We are more interested in if the pressing process can be applicable for large scale devices. A 0.5 cm^2 device has been selected, and the relating PCEs are recorded in Figure 4a,b and Tables S3 and S4. The control process only exhibited a PCE of 5.13%, whereas this has been increased to 6.02% in the pressing-assisted process. The hot-pressing process further promotes the PCE to 6.93% with a J_{SC} of 6.72 mA cm^{-2}, V_{OC} of 1.37 V, and FF of 0.76. This is about 30% higher than that of the control process. The results suggest that the hot-pressing process is more effective for large-scale devices. It is more interesting to note that the PCE of the pressing-treated PSCs dropped after 24 h of storage, whereas the PCE for the hot-pressing-treated PSCs remained almost constant during a 24 h storage (Figure 4). The influence of the applied pressure on the PCE of large-scale devices is listed in Figure S4 and Table S5, and the value of the optimum pressure is 32 N cm^{-2}. The achievable PCE first rises with the increased pressure, possibly due to a better contact. Meanwhile, further increasing the pressure introduces current leakage, which is detrimental for photo-carrier transportation. Besides, the PCE of large-scale devices with an active area of 1.02 cm^2 has been provided in Figure S5 and Table S6. The hot-pressing-treated device shows a PCE of 6.10%, which is nearly 30% higher than that of the control process.

To offer a better insight into the performance improvement caused by hot-pressing, the interfacial charge transfer and recombination dynamics are investigated. Figure 5a records the steady-state photoluminescence (PL) spectrum of the neat $CsPbBr_3$, $CsPbBr_3$/carbon, and hot-pressing $CsPbBr_3$/carbon films. The PL spectrum peaked at ∼530 nm, pointing to the formation of $CsPbBr_3$. Compared with the neat perovskite films, the PL intensity of the carbon-coated perovskite films has been greatly reduced (Figure 5a). This is due to an effective carrier transportation from the perovskite layer up to the carbon-carrier collection layer. Besides, the lower the PL intensity, the more effective the carrier transportation.[4,44] The hot-pressing process quenched the PL intensity to less than 1/2 of the initial intensity (perovskite/carbon film), supporting a better contact at the perovskite/carbon interface after hot-pressing. Meanwhile, for the time-resolved photoluminescence (TRPL) characterization, Figure 5b records the TRPL spectroscopy of the prepared films, the curves are fitted with a biexponential decay model of $I = Ae - (t - t_0)/\tau_1 + Be - (t - t_0)/\tau_2$, and the carrier lifetime is extracted as summarized in Table S7. Because a carrier-selective layer has been introduced, the faster component (τ_1) can be assigned to the photo-carrier transportation, and the long lifetime τ_2 can be considered the intrinsic radiative recombination. The average carrier lifetime (τ_{ave}), which can be calculated by deriving the formula of $\tau_{ave} = (a_1\tau_1^2 + a_2\tau_2^2)/(a_1\tau_1 + a_2\tau_2)$, has been calculated to evaluate the charge extraction ability. The τ_{ave} of the $CsPbBr_3$/FTO substrate without the carbon layer is approximately 7.61 ns, whereas the introduction of the carbon layer contributes to a reduced τ_{ave}, and the hot-pressing device shows a faster PL decay, indicating an enhanced hole extraction.

Furthermore, the $J-V$ characterization of various PSCs with a symmetric structure of FTO/$CsPbBr_3$/carbon is tested under

https://doi.org/10.1021/acsomega.1c06108
ACS Omega 2022, 7, 16877−16883

the dark condition (Figure 5c). A relatively lower dark current density has been identified in the hot-pressing device, which supports a reduction in charge recombination.[30,32,42] Apparently, the reduced carrier recombination is mainly due a better contact of the perovskite/carbon interface. Next comes to the electrochemical impedance spectra (EIS) characterization. In the dark with an applied bias of 0 V, the arc on the EIS spectrum can be assigned to the recombination resistance (R_r) of the device.[26] Here, *Rr* has been increased from 1.786 MΩ for the control device to 3.228 MΩ of the hot-pressing device (Figure 5d), further supporting a less possibility of carrier recombination in the hot-pressing device. Finally, the hot-pressing devices retain over 95% of their initial PCE after a 30 day-aging test (Figure S6), compared with 92% for the control device; thus, a better stability can be guaranteed.

CONCLUSIONS

To sum up, high performance and large-scale $CsPbBr_3$ PSCs are prepared via introducing a simple hot-pressing process. The hot-pressing process improves the contact at the perovskite/carbon interface and contributes to a better carrier transportation. Via adjusting the applied pressure, a superior PCE of 8.34% has been achieved for the hot-pressing-assisted device in comparison with 7.40% (pristine) and 7.95% (pressing devices). More importantly, the PCE of large-scale devices received a ∼30% PCE improvement (from 5.1% to 6.9%) with the hot-pressing treatment, indicating a more effective effect for large area devices. Furthermore, the hot-pressing devices showed an enhanced reproducibility and stability. Overall, the hot-pressing method shows broad prospects for carbon-based PSCs, especially for large-scale PSCs.

EXPERIMENTAL SECTION

Materials. The SnO_2 colloid precursor was purchased from Alfa Aesar (tin(IV) oxide). *N*,*N*-Dimethylformamide (DMF) was purchased from J&K Chemicals. Lead bromide ($PbBr_2$, 99.0%) and cesium bromide (CsBr, 99.9%) were obtained from Xi'an Polymer Light Technology Corp. The commercial carbon paste (including graphene and carbon black) was purchased from Shanghai Mater Win New Materials Co., Ltd. The other materials if not stated were purchased from TCI. All materials were used without further purification.

Device Fabrication. All the devices were prepared in the atmosphere environment. Fluorine-doped tin oxide (FTO) glasses were washed with detergent, deionized water, acetone, and isopropyl alcohol (IPA) in sequence for 15 min. The as-cleaned FTO was treated with UV-Ozone before use. As previously reported,[45] the Li-doped SnO_2 precursor solution was obtained by mixing SnO_2 (450 μL) colloid dispersion and LiCl (300 μL) aqueous solution (17 mg/4 mL) with water (2 mL). A thin SnO_2 layer was spin-coated onto the as-cleaned FTO at a speed of 4000 rpm for 30 s and annealed at 160 °C for 30 min. The $CsPbBr_3$ films were prepared with a modified method based on the multi-step spin-coating method reported by Tang et al.[40] In detail, the $PbBr_2$/DMF solution (1.0 M) was stirred at 70 °C for 30 min before being spin-coated onto the SnO_2 layer at a speed of 2000 rpm for 30 s. The substrates were preheated at 90 °C prior to spin coating. The prepared $PbBr_2$ films were annealed at 90 °C for 40 min. After cooling down, 0.07 M CsBr methanol solution was spin-coated onto the $PbBr_2$ film at 2000 rpm for 30 s and heated at 250 °C for 5 min. This process was repeated several times to fabricate the cesium lead bromide films. The obtained perovskite films were soaked in isopropanol for 30 min and dried at 250 °C again for 5 min. Finally, a carbon back-electrode was deposited on the perovskite film by the doctor-blade coating method. For the pressing device, the as-prepared device was placed glass face up on a flat table, with a flexible polytetrafluoroethylene (PTFE) thin film sandwiched between the carbon film and table as a buffer layer. Then, weights were added to the top of the glass to apply pressure. For the fabrication of hot-pressing PSCs, the coated carbon paste was heated at 100 °C for 5 min.

Characterizations and Measurements. The XRD patterns of the samples were measured on an Ultima IV X-ray diffractometer with Cu Kα radiation. The *J*−*V* curves and EIS data were collected with an electrochemical workstation (CHI-760). The morphologies of the perovskite films were recorded on a JSM-6510A SEM instrument. The UV−vis absorption spectra were measured with a Hitachi U-3900 instrument. Steady-state PL (excitation at 400 nm) was measured with an Edinburgh Instruments Ltd. instrument (FLS980). TRPL was measured on an FL980 with the time-correlated single photon counting method by excitation with a 405 nm laser.

ASSOCIATED CONTENT

Supporting Information

The Supporting Information is available free of charge at https://pubs.acs.org/doi/10.1021/acsomega.1c06108.

XRD patterns and UV−vis spectrum for the $CsPbBr_3$ films; *J*−*V* curves and stability of the as-prepared PSCs; photovoltaic parameters and TRPL time constant (PDF)

AUTHOR INFORMATION

Corresponding Authors

Teng Zhang − *School of Materials Science and Engineering, China University of Petroleum (East China), Qingdao 266580, P. R. China*; orcid.org/0000-0002-6555-9177; Email: tzhangae@connect.ust.hk

Xiyou Li − *School of Materials Science and Engineering, China University of Petroleum (East China), Qingdao 266580, P. R. China*; orcid.org/0000-0003-2548-2053; Email: xiyouli@upc.edu.cn

Authors

Chengben Liu − *College of Science, China University of Petroleum (East China), Qingdao 266580, P. R. China*

Zhi Li − *Shandong Energy Group Co., Ltd., Jinan City, Shandong Province 250014, China*

Baohua Zhao − *School of Materials Science and Engineering, China University of Petroleum (East China), Qingdao 266580, P. R. China*

Youru Bai − *School of Materials Science and Engineering, China University of Petroleum (East China), Qingdao 266580, P. R. China*

Xinmei Li − *School of Materials Science and Engineering, China University of Petroleum (East China), Qingdao 266580, P. R. China*

Wenwen Liu − *School of Materials Science and Engineering, China University of Petroleum (East China), Qingdao 266580, P. R. China*

https://doi.org/10.1021/acsomega.1c06108
ACS Omega 2022, 7, 16877−16883

Yanli Chen − *School of Materials Science and Engineering, China University of Petroleum (East China), Qingdao 266580, P. R. China;* orcid.org/0000-0003-3252-7889
Zhaobin Liu − *Shandong Energy Group Co., Ltd., Jinan City, Shandong Province 250014, China*

Complete contact information is available at: https://pubs.acs.org/10.1021/acsomega.1c06108

Author Contributions

#T. Z. and C. L. contributed equally to this work.

Notes

The authors declare no competing financial interest.

■ ACKNOWLEDGMENTS

Financial support from the National Natural Science Foundation of China (no. 22109179), Natural Science Foundation of Shandong Province (ZR2017MB006, ZR2017ZB0315, and ZR2017BB027), Fundamental Research Funds for the Central Universities (18CX02052A, 18CX02053A, and 20CX06004A), and Talent Introduction Program of China University of Petroleum (East China) (ZX20190162) is acknowledged. We also thank the support from the Yankuang Group 2019 Science and Technology Program (YKKJ2019AJ05JG-R60). X.L. and T.Z. thank the Taishan Scholar program of Shandong Province (ts201712019 and tsnq201909069) for financial support.

■ REFERENCES

(1) Zhang, T.; Hu, C.; Yang, S. Ion Migration: A "Double-Edged Sword" for Halide-Perovskite-Based Electronic Devices. *Small Methods* **2020**, *4*, 1900552.
(2) Mohd Yusoff, A. R. b.; Vasilopoulou, M.; Georgiadou, D. G.; Palilis, L. C.; Abate, A.; Nazeeruddin, M. K. Passivation and Process Engineering Approaches of Halide Perovskite Films for High Efficiency and Stability Perovskite Solar Cells. *Energy Environ. Sci.* **2021**, *14*, 2906−2953.
(3) Chen, S.; Dai, X.; Xu, S.; Jiao, H.; Zhao, L.; Huang, J. Stabilizing Perovskite-Substrate Interfaces for High-Performance Perovskite Modules. *Science* **2021**, *373*, 902−907.
(4) Zhao, B.; Yan, X.; Zhang, T.; Ma, X.; Liu, C.; Liu, H.; Yan, K.; Chen, Y.; Li, X. Introduction of Multifunctional Triphenylamino Derivatives at the Perovskite/HTL Interface To Promote Efficiency and Stability of Perovskite Solar Cells. *ACS Appl. Mater. Interfaces* **2020**, *12*, 9300−9306.
(5) Li, N.; Niu, X.; Li, L.; Wang, H.; Huang, Z.; Zhang, Y.; Chen, Y.; Zhang, X.; Zhu, C.; Zai, H.; Bai, Y.; Ma, S.; Liu, H.; Liu, X.; Guo, Z.; Liu, G.; Fan, R.; Chen, H.; Wang, J.; Lun, Y.; Wang, X.; Hong, J.; Xie, H.; Jakob, D. S.; Xu, X. G.; Chen, Q.; Zhou, H. Liquid Medium Annealing for Fabricating Durable Perovskite Solar Cells with Improved Reproducibility. *Science* **2021**, *373*, 561−567.
(6) Mei, A.; Li, X.; Liu, L.; Ku, Z.; Liu, T.; Rong, Y.; Xu, M.; Hu, M.; Chen, J.; Yang, Y.; Grätzel, M.; Han, H. A Hole-Conductor−Free, Fully Printable Mesoscopic Perovskite Solar Cell with High Stability. *Science* **2014**, *345*, 295−298.
(7) Wei, Z.; Yan, K.; Chen, H.; Yi, Y.; Zhang, T.; Long, X.; Li, J.; Zhang, L.; Wang, J.; Yang, S. Cost-Efficient Clamping Solar Cells using Candle Soot for Hole Extraction from Ambipolar Perovskites. *Energy Environ. Sci.* **2014**, *7*, 3326−3333.
(8) Duan, M.; Rong, Y.; Mei, A.; Hu, Y.; Sheng, Y.; Guan, Y.; Han, H. Efficient Hole-Conductor-Free, Fully Printable Mesoscopic Perovskite Solar Cells with Carbon Electrode Based on Ultrathin Graphite. *Carbon* **2017**, *120*, 71−76.
(9) Bogachuk, D.; Tsuji, R.; Martineau, D.; Narbey, S.; Herterich, J. P.; Wagner, L.; Suginuma, K.; Ito, S.; Hinsch, A. Comparison of Highly Conductive Natural and Synthetic Graphites for Electrodes in Perovskite Solar Cells. *Carbon* **2021**, *178*, 10−18.
(10) Duan, M.; Tian, C.; Hu, Y.; Mei, A.; Rong, Y.; Xiong, Y.; Xu, M.; Sheng, Y.; Jiang, P.; Hou, X.; Zhu, X.; Qin, F.; Han, H. Boron-Doped Graphite for High Work Function Carbon Electrode in Printable Hole-Conductor-Free Mesoscopic Perovskite Solar Cells. *ACS Appl. Mater. Interfaces* **2017**, *9*, 31721−31727.
(11) Jiang, P.; Jones, T. W.; Duffy, N. W.; Anderson, K. F.; Bennett, R.; Grigore, M.; Marvig, P.; Xiong, Y.; Liu, T.; Sheng, Y.; Hong, L.; Hou, X.; Duan, M.; Hu, Y.; Rong, Y.; Wilson, G. J.; Han, H. Fully Printable Perovskite Solar Cells with Highly-Conductive, Low-Temperature. *Perovskite-Compatible Carbon Electrode. Carbon* **2018**, *129*, 830−836.
(12) Li, H.; Cao, K.; Cui, J.; Liu, S.; Qiao, X.; Shen, Y.; Wang, M. 14.7% Efficient Mesoscopic Perovskite Solar Cells Using Single Walled Carbon Nanotubes/ Carbon Composite Counter Electrodes. *Nanoscale* **2016**, *8*, 6379−6385.
(13) Zhang, N.; Guo, Y.; Yin, X.; He, M.; Zou, X. Spongy Carbon Film Deposited on A Separated Substrate as Counter Electrode for Perovskite-Based Solar Cell. *Mater. Lett.* **2016**, *182*, 248−252.
(14) Gholipour, S.; Correa-Baena, J.-P.; Domanski, K.; Matsui, T.; Steier, L.; Giordano, F.; Tajabadi, F.; Tress, W.; Saliba, M.; Abate, A.; Morteza Ali, A.; Taghavinia, N.; Grätzel, M.; Hagfeldt, A. Highly Efficient and Stable Perovskite Solar Cells based on a Low-Cost Carbon Cloth. *Adv. Energy Mater.* **2016**, *6*, 1601116.
(15) Ye, T.; Hou, Y.; Nozariasbmarz, A.; Yang, D.; Yoon, J.; Zheng, L.; Wang, K.; Wang, K.; Ramakrishna, S.; Priya, S. Cost-Effective High-Performance Charge-Carrier-Transport-Layer-Free Perovskite Solar Cells Achieved by Suppressing Ion Migration. *ACS Energy Lett.* **2021**, *6*, 3044−3052.
(16) Yang, F.; Dong, L.; Jang, D.; Saparov, B.; Tam, K. C.; Zhang, K.; Li, N.; Brabec, C. J.; Egelhaaf, H.-J. Low Temperature Processed Fully Printed Efficient Planar Structure Carbon Electrode Perovskite Solar Cells and Modules. *Adv. Energy Mater.* **2021**, *11*, 2101219.
(17) Best Research-Cell Efficiency Chart.pdf; This Plot is Courtesy ofthe National Renewable Energy Laboratory: Golden, CO, available. https://www.nrel.gov/pv/cell-efficiency.html (accessed October 2021).
(18) Chen, H.; Yang, S. Carbon-Based Perovskite Solar Cells without Hole Transport Materials: The Front Runner to the Market? *Adv. Mater.* **2017**, *29*, 1603994.
(19) Zhu, H.; Liu, A.; Luque, H. L.; Sun, H.; Ji, D.; Noh, Y.-Y. Perovskite and Conjugated Polymer Wrapped Semiconducting Carbon Nanotube Hybrid Films for High Performance Transistors and Phototransistors. *ACS Nano* **2019**, *13*, 3971−3981.
(20) Wei, Z.; Chen, H.; Yan, K.; Zheng, X.; Yang, S. Hysteresis-Free Multi-Walled Carbon Nanotube-Based Perovskite Solar Cells with A High Fill Factor. *J. Mater. Chem. A* **2015**, *3*, 24226−24231.
(21) Ding, J.; Duan, J.; Guo, C.; Tang, Q. Toward Charge Extraction in All-Inorganic Perovskite Solar Cells by Interfacial Engineering. *J. Mater. Chem. A* **2018**, *6*, 21999−22004.
(22) Xu, H.; Duan, J.; Zhao, Y.; Jiao, Z.; He, B.; Tang, Q. 9.13%-Efficiency and Stable Inorganic $CsPbBr_3$ solar cells. Lead-free $CsSnBr_{3-x}I_x$ Quantum Dots Promote Charge Extraction. *J. Power Sources* **2018**, *399*, 76−82.
(23) Zhao, Y.; Duan, J.; Yuan, H.; Wang, Y.; Yang, X.; He, B.; Tang, Q. Using SnO_2 QDs and $CsMBr_3$ (M = Sn, Bi, Cu) QDs as Charge-Transporting Materials for 10.6%-Efficiency All-Inorganic $CsPbBr_3$ Perovskite Solar Cells with an Ultrahigh Open-Circuit Voltage of 1.610 V. *Solar RRL* **2019**, *3*, 1800284.
(24) Li, Q.; Bai, J.; Zhang, T.; Nie, C.; Duan, J.; Tang, Q. CdZnSe@ ZnSe Colloidal Alloy Quantum Dots for High-Efficiency All-Inorganic Perovskite Solar Cells. *Chem. Commun.* **2018**, *54*, 9575−9578.
(25) Liu, T.; Wang, Z.; Lou, L.; Xiao, S.; Zheng, S.; Yang, S. Interfacial Post-Treatment for Enhancing the Performance of Printable Carbon-Based Perovskite Solar Cells. *Solar RRL* **2020**, *4*, 1900278.
(26) Li, X.; Tan, Y.; Lai, H.; Li, S.; Chen, Y.; Li, S.; Xu, P.; Yang, J. All-Inorganic $CsPbBr_3$ Perovskite Solar Cells with 10.45% Efficiency

by Evaporation-Assisted Deposition and Setting Intermediate Energy Levels. *ACS Appl. Mater. Interfaces* **2019**, *11*, 29746−29752.
(27) Chen, T.; Tong, G.; Xu, E.; Li, H.; Li, P.; Zhu, Z.; Tang, J.; Qi, Y.; Jiang, Y. Accelerating Hole Extraction by Inserting 2D Ti_3C_2-MXene Interlayer to All Inorganic Perovskite Solar Cells with Long-Term Stability. *J. Mater. Chem. A* **2019**, *7*, 20597−20603.
(28) Zhao, Y.; Liu, T.; Ren, F.; Duan, J.; Wang, Y.; Yang, X.; Li, Q.; Tang, Q. Organic Hole-Transporting Materials for 9.32%-Efficiency and Stable $CsPbBr_3$ Perovskite Solar Cells. *Mater. Chem. Front.* **2018**, *2*, 2239−2244.
(29) Liu, Z.; Sun, B.; Liu, X.; Han, J.; Ye, H.; Shi, T.; Tang, Z.; Liao, G. Efficient Carbon-Based $CsPbBr_3$ Inorganic Perovskite Solar Cells by Using Cu-Phthalocyanine as Hole Transport Material. *Nano-Micro Lett.* **2018**, *10*, 34.
(30) Sun, M.; Zhu, J.; He, B.; Bu, F.; Ti, J.; Yao, X.; Chen, H.; Duan, Y.; Tang, Q. Efficient Defect Passivation and Charge Extraction with Hexamethylenetetramine Interface Modification for Hole-Transporting Layers-Free $CsPbBr_3$ Perovskite Solar Cells. *Solar RRL* **2021**, *5*, 2100344.
(31) Zhang, W.; Liu, X.; He, B.; Gong, Z.; Zhu, J.; Ding, Y.; Chen, H.; Tang, Q. Interface Engineering of Imidazolium Ionic Liquids toward Efficient and Stable $CsPbBr_3$ Perovskite Solar Cells. *ACS Appl. Mater. Interfaces* **2020**, *12*, 4540−4548.
(32) Bu, F.; He, B.; Ding, Y.; Li, X.; Sun, X.; Duan, J.; Zhao, Y.; Chen, H.; Tang, Q. Enhanced energy level alignment and hole extraction of carbon electrode for air-stable hole-transporting material-free $CsPbBr_3$ perovskite solar cells. *Sol. Energy Mater. Sol. Cells* **2020**, *205*, 110267.
(33) Duan, J.; Wang, Y.; Yang, X.; Tang, Q. Alkyl-Chain-Regulated Charge Transfer in Fluorescent Inorganic $CsPbBr_3$ Perovskite Solar Cells. *Angew. Chem., Int. Ed.* **2020**, *59*, 4391−4395.
(34) Ding, J.; Zhao, Y.; Duan, J.; He, B.; Tang, Q. Alloy-Controlled Work Function for Enhanced Charge Extraction in All-Inorganic $CsPbBr_3$ Perovskite Solar Cells. *ChemSusChem* **2018**, *11*, 1432−1437.
(35) Mi, L.; Zhang, Y.; Chen, T.; Xu, E.; Jiang, Y. Carbon Electrode Engineering for High Efficiency All-Inorganic Perovskite Solar Cells. *RSC Adv.* **2020**, *10*, 12298−12303.
(36) Zhao, Y.; Zhu, J.; He, B.; Tang, Q. Enhanced Hole Extraction by Electron-Rich Alloys in All-Inorganic $CsPbBr_3$ Perovskite Solar Cells. *Chem. Commun.* **2021**, *57*, 7577−7580.
(37) Zhou, Q.; Duan, J.; Yang, X.; Duan, Y.; Tang, Q. Interfacial Strain Release From the $WS_2/CsPbBr_3$ Van Der Waals Heterostructure for 1.7 V Voltage All Inorganic Perovskite Solar Cells. *Angew. Chem., Int. Ed.* **2020**, *59*, 21997−22001.
(38) Zhou, Q.; Duan, J.; Du, J.; Guo, Q.; Zhang, Q.; Yang, X.; Duan, Y.; Tang, Q. Tailored Lattice "Tape" to Confine Tensile Interface for 11.08%-Efficiency All-Inorganic $CsPbBr_3$ Perovskite Solar Cell with an Ultrahigh Voltage of 1.702 V. *Adv. Sci.* **2021**, *8*, 2101418.
(39) Zhang, W.; Liu, X.; He, B.; Zhu, J.; Li, X.; Shen, K.; Chen, H.; Duan, Y.; Tang, Q. Enhanced Efficiency of Air-Stable $CsPbBr_3$ Perovskite Solar Cells by Defect Dual Passivation and Grain Size Enlargement with a Multifunctional Additive. *ACS Appl. Mater. Interfaces* **2020**, *12*, 36092−36101.
(40) Duan, J.; Zhao, Y.; He, B.; Tang, Q. High-Purity Inorganic Perovskite Films for Solar Cells with 9.72% Efficiency. *Angew. Chem., Int. Ed.* **2018**, *57*, 3787−3791.
(41) Zhao, Y.; Duan, J.; Wang, Y.; Yang, X.; Tang, Q. Precise Stress Control of Inorganic Perovskite Films for Carbon-Based Solar Cells with An Ultrahigh Voltage of 1.622 V. *Nano Energy* **2020**, *67*, 104286.
(42) Zhou, Q.; Du, J.; Duan, J.; Wang, Y.; Yang, X.; Duan, Y.; Tang, Q. Photoactivated Transition Metal Dichalcogenides to Boost Electron Extraction for All-inorganic Tri-brominated Planar Perovskite Solar Cells. *J. Mater. Chem. A* **2020**, *8*, 7784−7791.
(43) Wang, K.; Zheng, L.; Zhu, T.; Yao, X.; Yi, C.; Zhang, X.; Cao, Y.; Liu, L.; Hu, W.; Gong, X. Efficient Perovskite Solar Cells by Hybrid Perovskites Incorporated with Heterovalent Neodymium Cations. *Nano Energy* **2019**, *61*, 352−360.
(44) Wang, G.; Dong, W.; Gurung, A.; Chen, K.; Wu, F.; He, Q.; Pathak, R.; Qiao, Q. Improving Photovoltaic Performance of Carbon-based $CsPbBr_3$ Perovskite Solar Cells by Interfacial Engineering Using P3HT Interlayer. *J. Power Sources* **2019**, *432*, 48−54.

https://doi.org/10.1021/acsomega.1c06108
ACS Omega 2022, 7, 16877−16883